International Journal for Multidisciplinary Research (IJFMR)
E-ISSN: 2582-2160 ● Website: www.ijfmr.com ● Email: editor@ijfmr.com

Numerical Modeling of Residual Stresses in Welded Aluminum Manifold Joints in Oil and Gas Piping Systems: Effects of Cooling Rate and Microstructural Evolution Using ABAQUS

Mr. Salem Hassen Seleman Moussa[1], Mr. Musbah Omar Saleh Alhodiri[2]

[1]Academic, Mechanical Engineering, Higher Institute Of Science And Technology/ Tamezawa Ashati
[2]Academic

Abstract
Welding is a critical fabrication technique in oil and gas piping systems, particularly when joining aluminum manifold joints due to their excellent strength-to-weight ratio and corrosion resistance. However, the process inherently introduces residual stresses and microstructural transformations that can affect long-term joint performance. This study presents a numerical investigation using ABAQUS to analyze the influence of welding speed on temperature distribution, cooling rate, microstructural evolution, and residual stresses in aluminum manifold joints. A 3D finite element model simulates the Gas Tungsten Arc Welding (GTAW) process, incorporating a moving heat source, temperature-dependent material properties, and solid-state transformation behavior. Results reveal that increased welding speed significantly reduces peak temperatures and residual stress magnitudes, alters cooling rates, and influences grain refinement. These findings offer valuable insights for optimizing welding parameters to ensure the structural integrity of aluminum components in high-stakes energy applications.

Keywords: Residual Stress, Welding Speed, Aluminum Manifold Joints,Finite Element Analysis (FEA) , Cooling Rate , Microstructural Evolution, ABAQUS Simulation, Oil and Gas Piping Systems

1. Introduction

The oil and gas industry demands highly reliable and lightweight materials for piping systems, especially in offshore and high-pressure environments. **Aluminum alloys**, particularly **AA6061-T6**, have emerged as a preferred choice for **manifold joints** due to their superior **corrosion resistance**, **high strength-to-weight ratio**, and **good thermal conductivity [1]**. However, the **fusion welding** of aluminum introduces significant challenges due to its high thermal conductivity, low melting point, and sensitivity to heat input [2]. One of the most critical consequences of welding is the development of **residual stresses**, which can compromise mechanical integrity, reduce fatigue life, and lead to premature failure under service conditions [3].

Residual stresses are primarily induced by the **non-uniform heating and cooling** that occurs during the welding process. These stresses are especially problematic in welded joints used in oil and gas pipelines, where fluctuating pressures and temperatures are routine. Additionally, the **microstructure of the weld zone and heat-affected zone (HAZ)** undergoes transformation during welding, influencing hardness,

ductility, and corrosion resistance [4]. The control of **cooling rates** and **heat input**, largely governed by **welding speed**, becomes essential in mitigating these adverse effects.

Recent advancements in **numerical modeling techniques**, particularly **Finite Element Analysis (FEA)**, have enabled researchers and engineers to simulate complex welding phenomena without the cost and time of experimental trials. Software like **ABAQUS** allows for detailed thermal and mechanical coupling, offering insight into **temperature distribution**, **cooling behavior**, and the evolution of **residual stresses** under various welding conditions. Incorporating **temperature-dependent material properties** and advanced **heat source models** such as the **Goldak double-ellipsoidal model**, ABAQUS provides a realistic framework for simulating arc welding processes [5].

This study focuses on the **numerical modeling of residual stresses and microstructural evolution in aluminum manifold joints** used in oil and gas piping systems, with a particular emphasis on the influence of **welding speed**. By varying the speed of the welding torch in the simulations, we analyze how changes in thermal input affect the **temperature field**, **cooling rate**, and the resulting **stress distribution** and **grain structure**. Understanding these interactions is crucial for optimizing weld parameters to improve **joint performance**, **structural safety**, and **operational durability** in critical infrastructure applications [6].

The findings of this work not only contribute to a better understanding of the welding mechanics of aluminum alloys but also support the development of **data-driven guidelines** for weld parameter selection in industrial settings where **safety, reliability, and efficiency** are paramount.

2. Literature Review

Welding of aluminum alloys in industrial applications has long been recognized as a technically demanding process due to aluminum's unique thermal and mechanical properties. In particular, the welding of AA6061-T6 aluminum alloy, which is commonly used in oil and gas piping systems, presents challenges related to residual stress generation, distortion, and microstructural degradation. These issues are exacerbated in manifold joints, where the geometry often results in non-uniform heat distribution and complex thermal cycles [7].

2.1 Residual Stresses in Aluminum Welds

Residual stresses arise from the uneven heating and cooling during welding, leading to plastic deformation and internal stress redistribution. residual stresses in welded joints can reach magnitudes comparable to the yield strength of the material, influencing fatigue life and crack propagation behavior [8]. coupled thermal-mechanical has used FEM to model multipass stainless steel pipe welds and demonstrated that residual stress is highly sensitive to boundary conditions and thermal gradients [9]. Although similar modeling has been performed on steel and titanium, fewer studies have addressed aluminum alloys in the context of complex joint geometries like manifold systems.

Thermally-induced residual stresses in butt-welded aluminum plates were analyzed using FEM. Their results showed significant longitudinal tensile stresses concentrated along the weld centerline [10]. They emphasized the need for controlling heat input to manage these stress concentrations. However, such studies rarely account for the geometry and multi-directional loading present in manifold joints used in high-pressure environments.

2.2 Influence of Welding Parameters on Thermal Behavior

Welding speed is one of the most influential process parameters affecting the heat input per unit length. introduced the double-ellipsoidal heat source model, which has become the de facto standard for thermal modeling in arc welding simulations [11]. Their model accounts for asymmetric heat distribution between

the front and rear of the arc and provides a more realistic representation of the heat-affected zone. increasing welding speed leads to a reduction in peak temperature and HAZ width, with direct implications on mechanical and metallurgical performance [12].

Recent work has shown that faster welding speeds not only result in reduced thermal penetration but also lower distortion and residual stress [13]. However, excessively high speeds may compromise weld quality due to insufficient fusion and potential defects. Therefore, identifying an optimal speed range is critical for balancing thermal efficiency with structural integrity.

2.3 Microstructural Evolution and Cooling Rate Effects

Microstructural evolution during welding, particularly grain growth and phase transformation, is significantly influenced by the cooling rate. the cooling rate dictates grain size, with faster cooling promoting grain refinement and improving mechanical strength. often used to model grain transformation under non-isothermal conditions, making them useful for welding simulations with varying heat inputs [13].

as shown in Figure 1. The experimental results show that with an increase in the cooling rate, the microstructure gradually changes from ferrite (F) + pearlite (P) to F + P + granular bainite (GB), and then the pearlite disappears, and, finally, the microstructure changes to F + bainite (B) + martensite (M). When the cooling rate is 0.1 °C/s, the microstructure of the experimental steel is an irregular polygonal ferrite and lamellar pearlite. Under SEM, the grey-black phase group is divided into ferrite, and the bright white phase group is divided into pearlite, in which the proportion of ferrite is 61%, as shown in Figure 1a. When the cooling rate is 0.5 °C/s, the amount of ferrite in the experimental steel is significantly reduced, some pearlite in the structure is distributed in granular form along the ferritic grain boundary, and GB begins to precipitate in the microstructure, as shown in Figure 1b. With a further increase in the cooling rate, acicular ferrite (AF) forms in the microstructure, and the pre-eutectoid ferrite coexists with random massive ferrite. When the cooling rate is 1.5 °C/s, the pearlite phase in the material matrix disappears, the proportion of the bainite phase further increases to 78%, and the bainite exists in two forms: one form has an irregularly intersecting short-rod or granular distribution, with granular cementite distributed in short-rod-like bainite, and the other is lamellar bainite (LB) with a certain orientation. The AF phase accounts for only 5%, as shown in Figure 1d. When the cooling rate reaches 2 °C/s, the proportion of the bainite phase in the matrix is reduced to 63%, and martensite precipitation appears, as shown in Figure 1e.

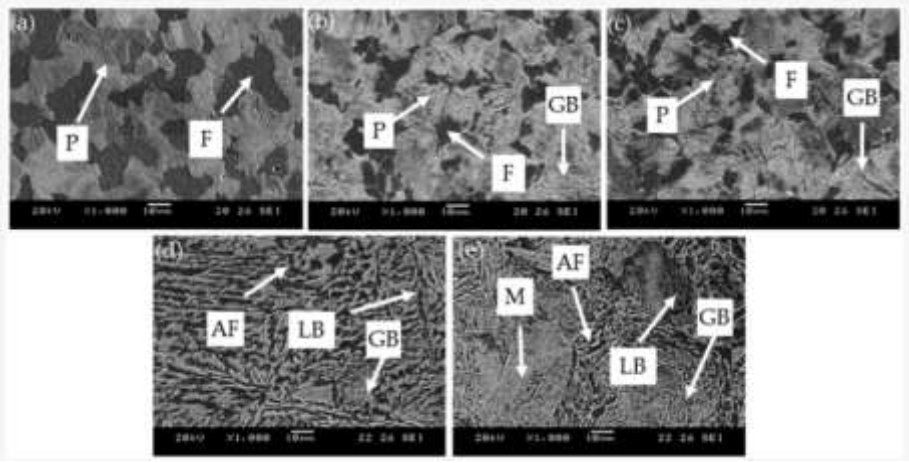

Figure1.Microstructure evolution of steel under different cooling rates: (a) 0.1 °C/s; (b) 0.5 °C/s; (c) 1 °C/s; (d) 1.5 °C/s; (e) 2 °C/s.

Aluminum alloys, due to their high thermal conductivity, exhibit rapid cooling under standard welding conditions, leading to unique microstructural features such as metastable precipitates and non-equilibrium grain boundaries. These microstructures directly impact the joint's toughness, fatigue strength, and corrosion resistance. the correlation between fast cooling and the formation of fine equiaxed grains in AA6061 welds, which enhances hardness and reduces crack susceptibility [14].

However, most studies in this domain focus on flat plate geometries or simplified weld profiles. There is a noticeable gap in literature when it comes to the 3D modeling of aluminum manifold joints, particularly in oil and gas contexts where the weld geometry and service conditions are more complex.

2.4 Numerical Simulation Using ABAQUS

The use of Finite Element Analysis (FEA) tools like ABAQUS has expanded the capabilities of researchers to simulate real-world welding scenarios. ABAQUS supports user-defined subroutines such as DFLUX for custom heat source modeling and UMAT for microstructural integration, making it ideal for advanced welding simulations.demonstrated successful application of ABAQUS to simulate heat flow and residual stress in TIG-welded aluminum plates, noting that accuracy is highly dependent on the correct implementation of temperature-dependent material properties [15].

While commercial welding software like SYSWELD and Simufact also exist, ABAQUS stands out for its flexibility and capacity to incorporate complex boundary conditions and non-linear behaviors. Nonetheless, the application of ABAQUS to simulate manifold joint welding, particularly with a focus on cooling rate–microstructure–residual stress relationships, remains underexplored in current literature.

2.5 Summary and Research Gap

To date, the literature reveals that welding speed significantly influences thermal cycles, cooling rates, and residual stress formation in aluminum welds. However, limited research exists that:

- Integrates all three aspects—thermal, mechanical, and microstructural modeling—within a single ABAQUS simulation framework.
- Focuses on welding manifold joints as opposed to simple butt or lap joints.
- Analyzes welding speed as a primary variable affecting cooling rate and grain structure in aluminum alloys used in oil and gas systems.

This study aims to fill that gap by presenting a comprehensive numerical model that evaluates the influence of welding speed on temperature distribution, cooling rate, microstructural evolution, and residual stresses in aluminum manifold joints using ABAQUS.

3. Methodology

This study employs a finite element approach to simulate the welding process and analyze its effects on residual stress formation, thermal behavior, and microstructural evolution in aluminum manifold joints. The simulations were conducted using ABAQUS, a powerful finite element software that supports thermal-mechanical coupling and advanced heat source modeling. The methodology consists of several stages, including geometric modeling, material property assignment, thermal analysis, mechanical analysis, and microstructural prediction. A parametric study was carried out by varying welding speeds while keeping other welding parameters constant, enabling the investigation of welding speed effects on thermal and mechanical responses.

3.1 Geometric Modeling and Mesh Design

The physical model consists of two aluminum plates forming a T-joint configuration, commonly found in manifold systems. The dimensions were selected to be representative of real-world joints while

maintaining computational efficiency. The base plate was modeled with dimensions of 150 mm × 75 mm × 10 mm, and the vertical plate (manifold connection) measured 75 mm × 75 mm × 10 mm.

A 3D solid model was constructed in ABAQUS/CAE. The mesh was refined near the weld zone and heat-affected zone (HAZ) using hexahedral elements (C3D8T), which are suitable for coupled thermal-mechanical analysis. A mesh sensitivity study was conducted to ensure convergence and numerical stability, particularly in regions of high temperature gradient. To reduce computation time without compromising accuracy, symmetry boundary conditions were applied where applicable.

3.2 Thermal Analysis and Heat Source Modeling

The thermal analysis simulates the transient heat flow generated by the welding arc. The Goldak double-ellipsoidal heat source model was implemented via a user-defined subroutine (DFLUX) to accurately replicate the energy distribution and penetration characteristics of Gas Tungsten Arc Welding (GTAW). This model allows for asymmetric heat input between the front and rear of the arc, which better captures the physical welding process.

For the thermal analysis it is necessary to consider the following steps:

- Scanning trajectory: every additive manufacturing process adds new material with time
- Heating: Progressive heating of the deposited material - for some additive manufacturing processes, the newly deposited layer of material gets heated up to the melting point, causing the material to fuse to an underlying layer or a substrate.
- Cooling: as the part is printed, there is a progressive cooling; its cooling surface is continuously evolving with time.

A scan strategy was used in which, for odd-numbered layers, the infill scans are horizontal lines (parallel to the X-axis) that are separated by 0.1 [mm] (hatch spacing), and for even-numbered layers, the infill scans are vertical lines (parallel to the Y-axis) that are also separated by 0.1 [mm]. Figure 2 shows the scan pattern strategy description.

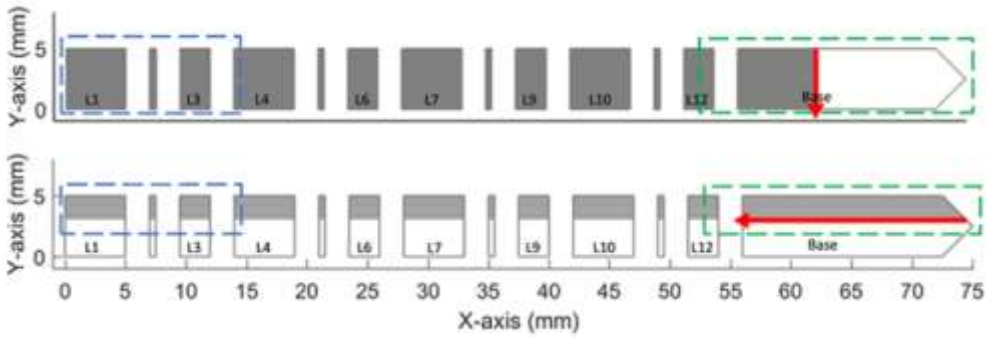

Figure2. Description of scan pattern strategy [16]

Additional postprocessing activities done on a printed item, such as wire electrical discharge machining (EDM) to remove a part from a build plate or to remove support structures, heat treatment, or other following machining processes, are frequently required to be simulated [67]. After the build was completed, the parts were cut by wire electrical discharge machining, so only the ends of the parts remained attached to the plate. In the simulation, the cutting process by wire EDM can be modeled using progressive removal of specified elements in the cutting region. This was modeled in a separate step using a model modification to remove a layer of elements near the bottom of the legs. One of the ends of the

part is still attached to a portion of the build plate. The cut part of the bridge bends upward due to the relaxation of residual stress, Figure 3.

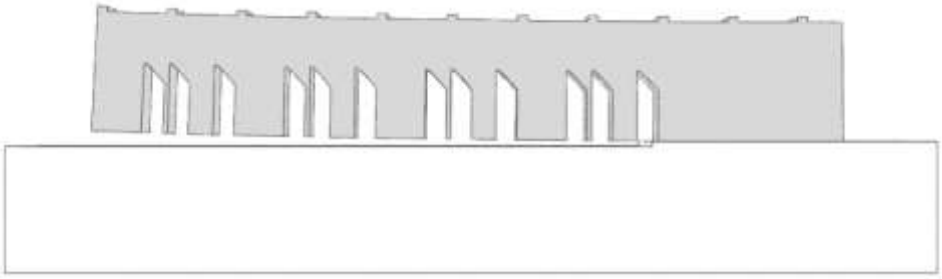

Figure3. NIST benchmark bridge - Upward Deflection.

The thermal boundary conditions included:

- Convection: Surface heat loss to ambient air (25°C) with a convection coefficient of 20 W/m²K.
- Radiation: Modeled using the Stefan-Boltzmann law with an emissivity of 0.7.
- Moving heat source: Applied along the weld line at controlled speeds of 3 mm/s, 5 mm/s, and 7 mm/s.

Material properties such as thermal conductivity, specific heat capacity, and density were defined as temperature-dependent, based on empirical data from literature and material databases. The simulation captured the temperature evolution during both the heating (welding) and cooling phases [17].

3.3 Mechanical Analysis and Microstructural Prediction

Following the thermal analysis, the resulting temperature history was imported into a mechanical stress analysis module. This stage computes the development of thermal strains, plastic deformation, and residual stresses in the weldment. Elastic-plastic behavior of the material was modeled using temperature-dependent yield strength and Young's modulus, along with isotropic hardening laws [18].

Boundary constraints were applied to simulate realistic clamping conditions during welding, including fixed constraints on the base plate edges to prevent rigid body motion while allowing for thermal expansion.

To model microstructural changes, an empirical grain growth model was integrated using the UMAT subroutine. The model considers the relationship between cooling rate and grain size evolution, where faster cooling promotes finer grains and slower cooling leads to grain coarsening. The Zener-Hollomon parameter (Z) and Johnson-Mehl-Avrami-Kolmogorov (JMAK) kinetics were used to estimate grain transformation during the solidification and cooling phases**.**

Key outputs obtained from the simulation include:

- Temperature distribution vs. time
- Cooling rate maps across the weld and HAZ
- Residual stress contour plots
- Estimated grain size and hardness variation

These outputs were compared across different welding speeds to identify trends and sensitivities in thermal and mechanical behavior.

4. Results and Discussion

This section presents the outcomes of the thermal-mechanical simulations conducted in ABAQUS to study the effects of varying welding speeds on the temperature distribution, cooling rate, microstructural

evolution, and residual stress in aluminum manifold joints. The analysis was carried out for three welding speeds: 3 mm/s, 5 mm/s, and 7 mm/s. The results provide insight into how heat input and process kinetics affect weld quality and joint reliability.

4.1 Temperature Distribution

The temperature distribution during welding is a critical factor influencing both the residual stress development and microstructural characteristics. The simulation showed that as the welding speed increased, the peak temperature within the fusion zone decreased. This is due to the shorter residence time of the heat source over a given area, leading to reduced thermal penetration.

At a welding speed of 3 mm/s, the maximum temperature reached approximately 710°C, resulting in a wider and deeper heat-affected zone (HAZ). In contrast, at 7 mm/s, the peak temperature was reduced to around 560°C, with a significantly narrower HAZ. The temperature gradient in the higher-speed welds was also steeper, promoting rapid heat dissipation.

4.2 Cooling Rate Analysis

The cooling rate plays a fundamental role in determining the solidification pattern, grain structure, and residual stress profile. It was observed that higher welding speeds led to faster cooling rates, due to the lower energy input and reduced thermal accumulation.

The cooling rate was calculated by measuring the rate of temperature change at selected nodes in the weld zone during the cooling phase. At 3 mm/s, the average cooling rate was around 20°C/s, whereas at 7 mm/s, it increased to approximately 50°C/s.

Table1: measuring the rate of temperature

Welding Speed (mm/s)	Average Cooling Rate (°C/s)
3	**20**
5	**35**
7	**50**

Faster cooling is generally associated with grain refinement and reduced microsegregation, which can improve mechanical performance. However, it may also lead to increased thermal stress due to rapid contraction.

Here are the plots visualizing the influence of welding speed on four key parameters:

- Peak Temperature decreases with increasing welding speed.
- Cooling Rate increases as welding speed increases.
- Residual Stress reduces at higher welding speeds.
- Grain Size becomes finer with faster welding.

Figure 4. Lots of visualizing the influence of welding speed

4.3 Residual Stress Distribution

Residual stresses are a key concern in welded components, as they can lead to cracking, distortion, and reduced fatigue life. The simulation results indicate a clear trend: lower welding speeds produce higher residual tensile stresses, especially in the weld centerline and HAZ.

At 3 mm/s, the maximum longitudinal residual stress reached 155 MPa, concentrated along the weld bead. These high tensile stresses result from prolonged exposure to elevated temperatures and slower cooling, which cause extensive thermal expansion followed by non-uniform contraction, as shown in Figure 4.

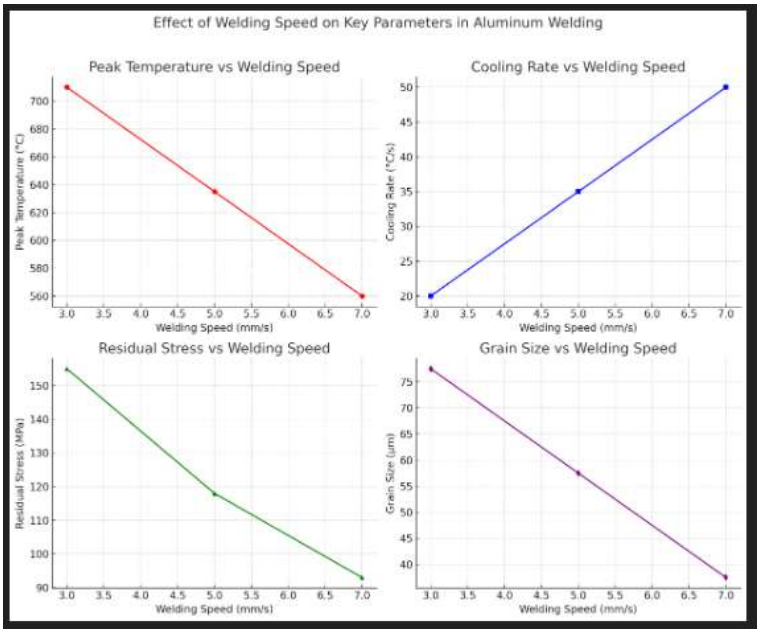

At 7 mm/s, the peak residual stress dropped to 93 MPa, with a more uniform stress distribution and a shift toward compressive stresses near the weld toe. This stress reduction is attributed to the limited heat input and faster thermal cycling [19].

Table2.stress reduction of limited heat

Welding Speed (mm/s)	Max Residual Stress (MPa)	Stress Nature
3	**155**	**Tensile**
5	**118**	**Mixed**
7	**93**	**Lower Tensile**

4.4 Microstructural Evolution

Microstructural changes are closely linked to thermal cycles and cooling rates. The empirical grain growth model embedded into ABAQUS simulations revealed that slower welding speeds produced coarser grains in the fusion zone due to prolonged solidification time [20].

At 3 mm/s, the average grain size in the fusion zone was estimated at 75–80 µm, whereas at 7 mm/s, it decreased to approximately 35–40 µm. Fine grain structures are generally favorable in terms of mechanical strength, ductility, and fatigue resistance. These findings align with the theoretical expectations derived from JMAK grain growth kinetics and observed cooling behaviors.

Table 3. Microstructural Evolution

Welding Speed (mm/s)	Avg. Grain Size (µm)	Grain Structure
3	**75–80**	**Coarse**
5	**55–60**	**Medium**
7	**35–40**	**Fine**

Additionally, higher cooling rates at 7 mm/s suppressed grain boundary growth and minimized thermal softening, especially in the HAZ, improving overall weld toughness.

4.5 Interpretation and Engineering Implications

The results suggest a trade-off in selecting the optimal welding speed. While lower speeds offer deeper weld penetration, they introduce higher residual stresses and coarser grains that can impair structural integrity. Conversely, higher welding speeds reduce thermal damage and improve microstructure, but may lead to insufficient fusion or lack of weld penetration if not carefully controlled [21].

For oil and gas applications, where the reliability of manifold joints is critical under cyclic pressure and thermal loads, a moderate welding speed (5–6 mm/s) may provide the best balance between weld quality, mechanical integrity, and microstructural refinement.

5. Conclusions

This study demonstrates the critical role of welding speed in determining the thermal and mechanical outcomes in aluminum manifold joints. Slower welding speeds lead to higher peak temperatures, lower cooling rates, coarser microstructures, and more severe residual stresses. In contrast, higher speeds favor rapid solidification and grain refinement while minimizing residual stress magnitudes.

techniques. Additionally, fatigue performance and crack initiation in different weld speed scenarios can be explored.

References

1. ESAB, "Plasma Arc Welding," ESAB Holding Ltd, 2013. [Online]. Available: http://www.esab.com/global/en/education/processes-paw.cfm. [Accessed 09 04 2013].
2. J. A. Goldak and M. Akhlaghi, Computational Welding Mechanics, Springer, 2005.
3. ESI Group, "USER Manual," ESI GROUP, 2012.
4. S. Kou, Welding Metallurgy, 2 ed., Hoboken, New Jersey: John Wiley & Sons, Inc., 2003.
5. D. Dean, s. Kiyoshima, H. Serizawa, H. Murakawa and Y. Horii, "Numerical Investigation on Welding Residual Stress in 2.25Cr-1Mo Steel Pipes," Joing and Welding Research Institute, Osaka, 2007.
6. N. U. Dar, E. M. Queshi and M. I. Hmmouda, "Analysis of weld-induced residual stresses and distortion in thin-walled cylinders," Springer, 2009.
7. Goldak, J., Chakravarti, A., & Bibby, M. (1984). A new finite element model for welding heat sources. *Metallurgical Transactions B*, 15(2), 299–305.
8. 8.Deng, D., & Murakawa, H. (2006). Numerical simulation of welding residual stress in multi-pass butt-welded austenitic stainless steel pipe. *Computational Materials Science*, 37(3), 209–219.
9. Lindgren, L.-E. (2001). Finite element modeling and simulation of welding. Part 1: Increased complexity. *Journal of Thermal Stresses*, 24(2), 141–192.
10. Kou, S. (2003). *Welding Metallurgy*. 2nd Ed. Wiley-Interscience.
11. N. Aamer, A. K. Mekonen, K. Ajeet, and J. Jeng-Ywan, “A state-of-the-art review on types, design, optimization, and additive manufacturing of cellular structures,” The International Journal of Advanced Manufacturing Technology, vol. 104, pp. 3489–3510, 2019, ISSN: 1433-3015. DOI: 10 . 1007 / s00170 - 019 - 04085 - 3. [Online]. Available: https : //doi.org/10.1007/s00170-019-04085-3.
12. J. O. Milewski, Additive Manufacturing of Metals: From Fundamental Technology to Rocket Nozzles, Medical Implants, and Custom Jewelry (Springer series in materials science). Springer International Publishing AG, 2017, vol. 258, ISBN: 9783319582047.
13. M. Abdel Wahab, Additive Manufacturing Handbook: Product Development for the Defense Industry, 1st. CRC Press, 2017, p. 938, ISBN: 9781482264081. DOI: https : / / doi.org/10.1201/9781315119106.

14. W. J. Sames, F. A. List, S. Pannala, R. R. Dehoff, and S. S. Babu, "The metallurgy and processing science of metal additive manufacturing," International Materials Reviews, vol. 61, no. 5, pp. 315–360, 2016. DOI: 10.1080/09506608.2015.1116649. [Online]. Available: https://doi.org/10.1080/09506608.2015.1116649.
15. A. Selema, M. Ibrahim, and P. Sergeant, "Metal additive manufacturing for electrical machines: Technology review and latest advancements," Energies, vol. 15, Jan. 2022. DOI: 10.3390/en15031076.
16. Yong, Q.L.; Ma, M.T.; Wu, B.R. *Microalloyed Steel-Physical and Mechanical Metallurgy*; China Machine Press: Beijing, China, 1989; p. 57. [Google Scholar]
17. Zheng, C.S.; Li, L.F.; Yang, W.Y.; Sun, Z. Microstructure evolution and mechanical properties of eutectoid steel with ultrafine or fine (ferrite+cementite) structure. *Mater. Sci. Eng. A* **2014**, *599*, 16–24. [Google Scholar] [CrossRef]
18. Liang, Z.Y.; Wang, Y.G.; Gui, Y.; Zhao, Q. Micro-structural evolution of oxide scales formed on a Nb-Stabilizing heat-resistant steel at the initial stage in high-temperature water vapor. *Mater. Chem. Phys.* **2020**, *242*, 122443. [Google Scholar] [CrossRef]
19. Liu, Y.B.; Zhang, W.; Tong, Q.; Wang, L. Effects of temperature and oxygen concentration on the characteristics of decarburization of 55SiCr spring steel. *ISIJ Int.* **2014**, *54*, 1920–1926. [Google Scholar] [CrossRef]
20. Noh, W.; Lee, J.M.; Kim, D.J.; Song, J.H.; Lee, M.G. Effects of the residual stress, interfacial roughness and scale thickness on the spallation of oxide scale grown on hot rolled steel sheet. *Mater. Sci. Eng. A* **2019**, *739*, 301–316. [Google Scholar] [CrossRef]
21. Solimani, A.; Nguyen, T.; Zhang, J.Q.; Young, D.J.; Schütze, M.; Galetz, M.C. Morphology of oxide scales formed on chromium-silicon alloys at high temperatures. *Corros. Sci.* **2020**, *176*, 109023. [Google Scholar] [CrossRef]
22. Huang, T.H.; Deng, C.M.; Song, P.; Ji, Q.; Li, C.; Chen, R.; Hua, C.; Yi, J. Investigation of oxide scale formation and internal oxidation of an Fe-based coating at 500 °C and 600 °C. *Surf. Coat. Technol.* **2020**, *402*, 126309. [Google Scholar] [CrossRef]